Analytic Power Factor Calculation for Vernier Machines with Concentrated Windings

Dominik Thyroff [1], Christoph Hittinger [1], Ingo Hahn [1]
[1]Institute of Electrical Drives and Machines. University of Erlangen-Nuremberg, Erlangen, Germany

***Abstract*— It is well-known that the power factor of Vernier machines is small compared to permanent magnet machines. However, the power factor equations already derived show a huge deviation to the finite-element analysis (FEA) when used for Vernier machines with concentrated windings. Therefore, this paper develops an analytic model to calculate the power factor of Vernier machines with concentrated windings and different numbers of flux modulating poles (FMPs) and stator slots. The established model bases on the winding function theory in combination with a magnetic equivalent circuit. Consequently, equations for the q- inductance and for the no-load back-EMF of the machine are derived, thus allowing the calculation of the power factor. Thereby, the model considers stator leakage effects, as they are crucial for a good power factor estimation. Comparing the results of the Vernier machine to those of a pm machine explains the decreased power factor of Vernier machines. In addition, a FEA confirms the results of the derived model.**

Keywords*— *power factor, Vernier machine, concentrated windings, analytic model, magnetic equivalent circuit, leakage

I. Introduction

Vernier machines offer a very high torque density at low rotor speeds. Therefore, they appear very attractive as direct drives [1]. Vernier machines achieve their high torque density due to the flux modulation of the magnetic field, as this offers a conceptual advantage in machine design compared to pm machines [1] - [4]. On the one hand, the modulation of the field reduces the rotor speed and on the other hand, the field modulation allows the usage of different numbers of pole-pairs in the rotor and the stator [2]. This offers a wide range of possible machine designs, as listed in [5]. It seems beneficial for the machine design to decouple the number of stator slots from the number of FMPs to use a concentrated winding scheme in the stator [2]. However, the disadvantage of Vernier machines is their low power factor [5] – [8]. Some authors conjecture a high flux leakage in the rotor as reason for the low power factor [5], [6]. Thereby, the already derived power factor equations in [5], [7] and [8] refer to Vernier machines, in which the number of stator slots equals the number of pole-pieces. In comparison with a FEA simulation, the results of these equations seem not to be appropriate and proper in case of a concentrated winding. Therefore, this paper investigates an analytic power factor equation for the Vernier machine with concentrated windings and different numbers of slots and pole-pieces. For this purpose, different calculation models of the q-inductance are compared to the FEA. In addition, also the back-EMF of the stator is determined using the winding function theory, and the power factor equation is derived. A comparison of the found equations with the ones of a permanent magnet machine clarifies the reasons of the decreased power factor. Finally, a FEA verifies the developed analytical model.

II. Machine Geometry & Phasor Diagram

A. Machine geometry

The investigated Vernier machine, shown in Fig. 1, exhibits a concentrated winding and different numbers of stator slots and FMPs [2], [5]. Moreover, the stator winding creates $p_s=3$ pole pairs. In contrast, the rotor generates $p_r=24$ pole pairs with surface mounted permanent magnets. Therefore, to produce torque $n_p=27$ FMPs are necessary [2].

B. Voltage equations and phasor diagram

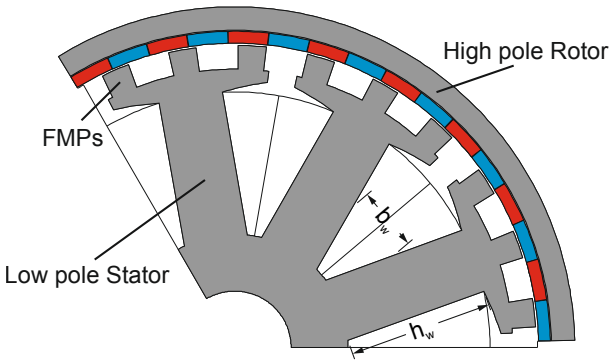

Fig. 1: Investigated Vernier machine

Table I Machine dimensions

Parameter	*Value in mm*
Stator yoke diameter	50
Stator diameter (without pole-pieces)	123
FMP height	5.25
Magnet height	2.61
Rotor height	5.15
Overall air-gap	0.75
Axial length	70

It is reasonable to assume that the voltage equation for the Vernier machine equals the one of the permanent magnet machine, since only the inductances and the no-load counter-

978-1-5090-4281-4/17/$31.00 ©2017 IEEE

electromotive force (back-EMF) will change. Thereby, to calculate the power factor, it is sufficient to focus on the mean values of the d- and q-inductance. Consequently, this approach omits the impact of higher rotor harmonics on the d- and q-inductance [9]. In Addition, assuming the absence of saturation induced saliencies allows modeling the machine with the stationary voltage equation for the base harmonic [9]:

$$\begin{bmatrix} u_d \\ u_q \end{bmatrix} = \begin{bmatrix} R_s & 0 \\ 0 & R_s \end{bmatrix} \begin{bmatrix} i_d \\ i_q \end{bmatrix} + \omega \begin{bmatrix} 0 & -L_q \\ L_d & 0 \end{bmatrix} \begin{bmatrix} i_d \\ i_q \end{bmatrix} + E_0 \begin{bmatrix} 0 \\ 1 \end{bmatrix} \quad (1)$$

Furthermore, Fig. 2 shows the phasor diagram according to the voltage equation (1) supposing the I_d=0 control strategy. Thus, applying trigonometric functions allows calculating the power factor of the Vernier machine:

$$\cos\varphi = \frac{R_s i_q + E_0}{U} = \frac{R_s i_q + E_0}{\sqrt{\left(\omega L_q i_q\right)^2 + \left(R_s i_q + E_0\right)^2}} = \frac{1}{\sqrt{\left(\frac{\omega L_q i_q}{R_s i_q + E_0}\right)^2 + 1}} \quad (2)$$

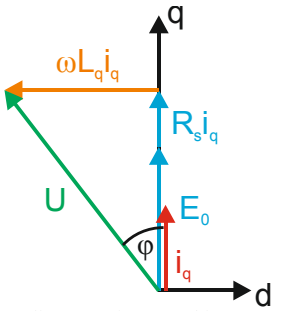

Fig. 2: Phasor diagram of pm machine controlled $I_d = 0$

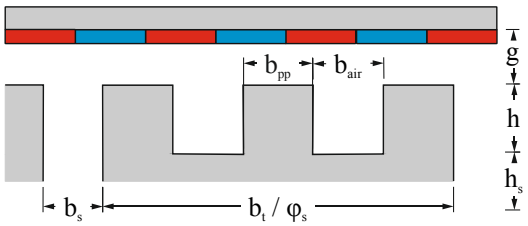

Fig. 3: Draft of geometric variables

Apparently, the calculation of the power factor requires the q-inductance and the no-load back-EMF (2). In a symmetric stator, the q-inductance equals 1.5 times the self-inductance, since the mutual inductance is the negative half of the self-inductance [9]. As the stator resistance is very small, it will be neglected in the further modeling process. Hence, to calculate the power factor, an accurate estimation of the self-inductance and the no-load back-EMF by the investigated machine model is necessary.

III. Machine Model

A. Air-gap permeance

In case of the permanent magnet machine, neglecting the stator and rotor slots leads to a constant air-gap permeance. In contrast, the air-gap permeance function of the Vernier machine equals to a rectangular function due to the FMPs in the air-gap. Therefore, it is possible to represent the permeance function as a Fourier series expansion according to the following expression:

$$\Lambda(\gamma) = \frac{\mu_0}{\delta(\gamma)} = \Lambda_0 + \sum_{k=1}^{\infty} \Lambda_k \cdot \cos(k p_p \gamma) \quad (3)$$

Thereby p_p denotes the number of FMPs in the airgap. The air-gap permeance function has a maximum value while a FMP element is present and a minimum value if there is no FMP present. In order to represent this behavior correctly it is necessary to choose the Fourier series parameters depending on the total air-gap length g and the height of the FMPs h:

$$\Lambda_0 = \frac{\mu_0}{g+h} + \frac{1}{2}\alpha_p \left(\frac{\mu_0}{g} - \frac{\mu_0}{g+h}\right) \quad (4)$$

$$\Lambda_k = \frac{2}{\pi}\left(\frac{\mu_0}{g} - \frac{\mu_0}{g+h}\right)\frac{1}{k}\sin\left(k\frac{\pi}{2}\alpha_p\right) \quad (5)$$

Whereby, α_p is the FMP width to the FMP pole pitch ratio and g considers the air-gap length including the height of the magnets. Thus, Fig. 1 and Fig. 3 illustrate the used geometric variables.

B. Self-inductance of the vernier machine with concentrated winding

In a first attempt, the winding function theory is utilized to calculate the self-inductance. Therefore, the air-gap flux density generated by one stator coil is required. Assuming the magneto motive force (MMF) of one stator coil as rectangular allows representing the stator MMF by a Fourier series expansion:

$$\Theta_S(\gamma) = \frac{2}{\pi} N_S i_s \sum_{k=1}^{\infty} \xi_{p_s} \cdot \cos(k p_s \gamma - k p_s \varphi_{ph}) \quad (6)$$

$$\xi_{p_s} = \frac{1}{k}\sin\left(k p_s \frac{\varphi_s}{2}\right) \quad (7)$$

Herein, N_s is the number of windings, i_s is the coil current, ξ_{ps} is the winding factor and φ_{ph} considers the phase shift. Since the higher harmonics introduced in the stator MMF and in the stator-sided air-gap permeance only increase the mean value of the self-inductance [9], the voltage equation for the base harmonic (1) is still valid. The air-gap flux density equals the multiplication of the stator MMF (6) with the permeance function (3):

$$B_S(\gamma) = \Lambda(\gamma) \cdot \Theta_S(\gamma) \tag{8}$$

Knowing the air-gap flux density allows determining the flux linkage with the excitation coil by integrating the flux density along one stator tooth. Furthermore, the self-inductance equals the total tooth flux linkage divided by the coil current:

$$\psi_{aa} = \frac{2}{\pi} N_s^2 l_{Fe} i_s R \cdot \left(\psi_{a,\Lambda_0} + \psi_{a,\Lambda_k}\right) \tag{9}$$

$$\psi_{a,\Lambda_0} = 2\Lambda_0 \sum_{k=1}^{\infty} \xi_{p_s}^2 \tag{10}$$

$$\psi_{a,\Lambda_k} = \sum_{k=1}^{\infty} \xi_{p_s} \Lambda_k \cdot \left(\frac{p_s}{p_p - p_s} \xi_{p_p - p_s} + \frac{p_s}{p_p + p_s} \xi_{p_p + p_s}\right) \tag{11}$$

$$L_{aa} = \frac{\psi_{aa}}{i_s} \tag{12}$$

Keeping the integration limits while moving the stator MMF (6) about φ_{ph} = 2/3π and 4/3π results the mutual flux linkage.

Thereby, the self-flux linkage of the Vernier machine (9) includes additional flux (11) in comparison to a pm machine. Furthermore, Λ_0 of the Vernier machine (4) is different to Λ_0 of the pm machine. Due to those differences, simply using the inductance formulas of a pm machine [5] is inappropriate for Vernier machines.

However, in comparison with a FEA, as presented in Fig. 4, the analytic model (12) shows rudimentary the same behavior, but results a much lower amplitude of the q-inductance. Apparently, Fig. 4 shows a constant offset between the analytic model and the FEA, indicating any kind of leakage flux as cause for the deviation. Unfortunately, the presented analytic model offers no possibility to consider leakage flux.

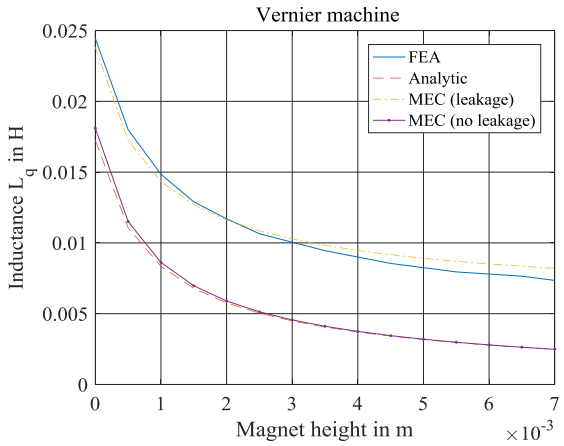

Fig. 4: Different models of the q-inductance for varying the magnet height

Therefore, Fig. 5 a) introduces a simple magnetic equivalent circuit (MEC) model of one stator pole pair to consider stator tooth leakage. Thereby, removing R_σ from the model results in a MEC model without leakage.

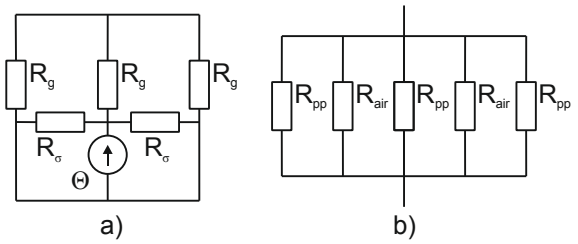

Fig. 5: a) MEC with stator leakage b) Composition of gap resistance R_g

According to Fig. 5 a) the total resistance

$$R = \frac{3}{2} R_g || R_\sigma || R_\sigma = \frac{\frac{3}{2} R_g \cdot R_\sigma}{R_\sigma + 3R_g} \tag{13}$$

of the MEC model is given due to a parallel connection of the leakage resistances R_σ with 1.5 times the gap resistance R_g. Furthermore, the gap resistance is a simplification of the airgap representation shown in Fig. 5 b):

$$R_g = \left(\frac{3}{R_{pp}} + \frac{2}{R_{air}}\right)^{-1} = \frac{R_{air} \cdot R_{pp}}{3R_{air} + 2R_{pp}} \tag{14}$$

Thereby the resistance

$$R_{air} = \frac{h + g}{\mu_0 b_{air} l_{Fe}} \tag{15}$$

represents the area between the FMPs, while the resistance

$$R_{pp} = \frac{g}{\mu_0 b_{pp} l_{Fe}} \tag{16}$$

characterizes the FMPs itself. Herein, b_{pp} equals the FMP width, b_{air} is the width between the FMPs and l_{Fe} is the axial length. The two-piece leakage resistance

$$R_\sigma = \frac{b_s}{\mu_0 (h + h_s) l_{Fe}} || \frac{b_w}{\mu_0 h_w l_{Fe}} \tag{17}$$

respects the parallel leakage paths of the neighboring FMPs, the slot opening and the winding area. Thereby, b_s is the slot opening width, h_s is the slot height, b_w is the average length of the winding area and h_w is the height of the stator tooth. Furthermore, dividing the MMF Θ by the total resistance (12) gives the tooth flux. Multiplying the flux with the number of turns N_s and the stator pole pair number p_s results the total tooth flux linkage:

$$\psi_{aa} = 2p_s N_s^2 i_s \mu_0 l_{Fe} \left(\frac{b_{pp}}{g} + \frac{\frac{2}{3} b_{air}}{g + h} + \frac{h + h_s}{b_s} + \frac{h_w}{b_w}\right) \tag{18}$$

Subsequently, the self-inductance is calculated according to (12).

In addition to the analytic model, Fig. 4 also shows results for the q-inductance gained by the MEC model. Thereby, Fig. 4 presents results of the MEC model with and without stator tooth leakage. However, the analytic model and the MEC model without leakage effects are in very good agreement while varying the magnet height. In contrast, using the MEC model with leakage effects shows a good agreement between the MEC

model and the FEA. Thus, the error in the analytic model results from the neglected stator leakage flux. In addition, Fig. 6 compares the different models of the q-inductance while varying the FMP height.

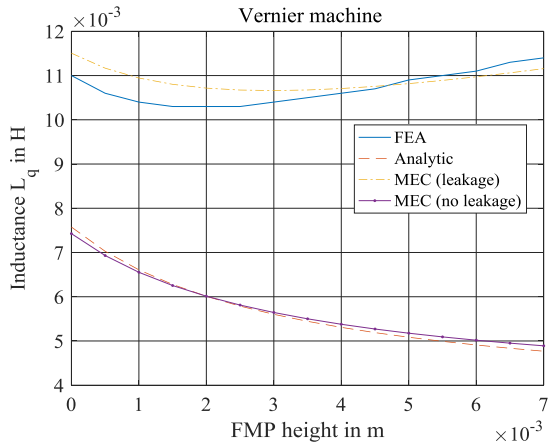

Fig. 6: Different models of the q-inductance for varying the FMP height

Thereby, the analytic model and the MEC model without leakage are again in very good agreement. However, Fig. 6 also shows a huge deviation between the analytic model and the FEA results. In contrast, the MEC model considering stator leakage approximates the FEA results clearly better. Thus, the MEC model considering stator leakage achieves a good representation of the q-inductance for simple airgap variations. The results presented in Fig. 4 and Fig. 6 highlight the influence of the stator leakage flux on the q-inductance. Due to the big influence on the q-inductance, a high impact of the leakage flux on the power factor is expected. Therefore, neglecting the leakage reactance [8] is inappropriate for Vernier machines with concentrated windings. In addition, Fig. 7 displays the differences between the q-inductance of the Vernier machine and the pm machine.

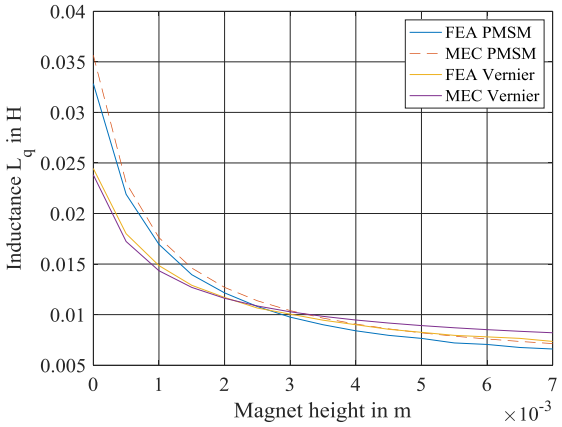

Fig. 7: Comparison of the q-inductance of Vernier and pm machine

Therein, the q-inductance of the Vernier machine is obviously smaller for thin magnets and slightly larger for thick magnets. However, due to the higher no-load back-EMF of the Vernier machine compared to a pm machine, [7] assumes a strong increase in the q-inductance of the Vernier machine to explain the poor power factor. Yet, Fig. 7 shows that this assumption is invalid, since the q-inductance of the Vernier machine is even smaller or only slightly bigger than for the pm machine.

C. *No-load back-EMF of the Vernier machine with concentrated windings*

The no-load back-EMF is determined in a similar way as described in [7]. Therefore, the magnet's MMF is modeled as rectangular function similar to (5). Furthermore the flux density is calculated by multipliyng the magnet's MMF with the permeance function (3). Integrating the flux density along the angular circumference of the stator φ_s and multiplying it with the axial length l_{Fe} of the machine gives the winding flux. Therefore, the back-EMF results by building the derivative of the flux along the position angle and afterwards multiplying the result with the mechanical speed:

$$E_0 = \frac{4}{\pi}\Theta_{Pm} N_s l_{Fe} \xi_{p_r} R \omega_{el} \sin(p_r \varphi_r) \cdot \left(2\Lambda_0 \xi_{p_r} \frac{p_s}{p_r} + \Lambda_1 \cdot \left(\xi_{p_s} + \frac{p_s}{(p_p+p_r)} \xi_{p_p+p_r}\right)\right) \quad (19)$$

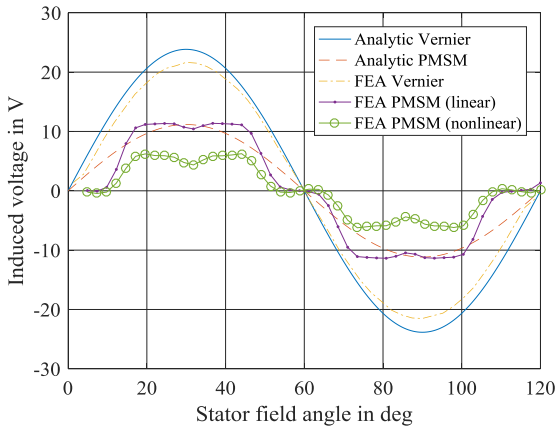

Fig. 8: Analytically calculated induced voltage in comparison to FEA

Furthermore, Fig. 8 shows the comparison of the presented back-EMF equation (19) with a FEA for the Vernier machine and for the pm machine. Thereby, using the simplifications $\Lambda_0 = \mu_0 / d$, $\Lambda_1 = 0$ and $p_r = p_s$ in the back-EMF equation and multiplying the resulting term with ξ_{ps} gives the back-EMF equation of the pm machine. In case of the Vernier machine (19) approximates the amplitude of the FEA in good accordance, whereas in case of the pm machine (19) only represents the correct amplitude when using linear materials. In this case, the rotor yoke of the pm machine saturates due to the clearly higher yoke flux of the pm machine compared to the Vernier machine. As the back-EMF equation (19) neglects the higher harmonics of the MMF, the resulting analytic waveforms are sinusoidal. Yet, offering a good approximation in case of the Vernier machine, as the FEA of the back-EMF also is sinusoidal. However, the estimation of the power factor only requires the amplitude of the back-EMF. Therefore, (19) is suitable for the power factor calculation of non-saturated Vernier and pm machines.

D. Power factor calculation

In contrast to the analytical models already derived [5], [7] and [8], III.B presents an analytical model for the q-inductance based on the winding function theory (12) for Vernier machines with concentrated windings. However, there is a huge deviation in the calculated q-inductance due to the neglected leakage flux. Yet, the calculated no-load back-EMF is in a very good agreement. Therefore, to increase the accuracy of the power factor calculation it is reasonable to use the introduced MEC model to calculate the q-inductance and the winding function theory to calculate the no-load back-EMF. Inserting both models in (2), offers an accurate analytical model of the power factor. Thereby, it is possible to fractionize the power factor equation (20) of the Vernier machine in four parts. Now K_{pm} (21) is the share of the pm machine without leakage, whereas $K_{pm,\sigma}$ (22) adds the leakage part of the pm machine. Furthermore, K_{Ve} (23) multiplies K_{pm} and considers the change in using a Vernier machine. In addition, $K_{Ve,\sigma}$ (24) multiplies $K_{pm,\sigma}$ and modifies the leakage share if using a Vernier machine.

$$\cos\varphi = \frac{1}{\sqrt{1+\left(K_{pm}K_{Ve}+K_{pm,\sigma}K_{Ve,\sigma}\right)^2}} \tag{20}$$

$$K_{pm} = \frac{p_s N_s i_s b_t}{\frac{8}{\pi}\Theta_{Pm}\xi_{p_s}\xi_{p_r}R} \tag{21}$$

$$K_{Ve} = \frac{\xi_{p_s}\frac{\mu_0}{b_t}\left(3\frac{b_{pp}}{g}+2\frac{b_{air}}{g+h}\right)}{\Lambda_0\frac{p_s}{p_r}\xi_{p_r}+\frac{1}{2}\Lambda_1\left(\xi_{p_s}+\frac{p_s}{p_p+p_r}\xi_{p_p+p_r}\right)} \tag{22}$$

$$K_{pm,\sigma} = \frac{3p_s N_s i_s g\left(\frac{h_s}{b_s}+\frac{h_w}{b_w}\right)}{\frac{8}{\pi}\Theta_{Pm}\xi_{p_s}\xi_{p_r}R} \tag{23}$$

$$K_{Ve,\sigma} = \frac{\xi_{p_s}\frac{\mu_0}{g}\cdot\frac{(h_s+h)b_w+h_w b_s}{h_s b_w+h_w b_s}}{\Lambda_0\frac{p_s}{p_r}\xi_{p_r}+\frac{1}{2}\Lambda_1\left(\xi_{p_s}+\frac{p_s}{p_p+p_r}\xi_{p_p+p_r}\right)} \tag{24}$$

Therefore, in case of the pm machine the power factor equation simplifies, as the Vernier machine coefficients are $K_{Ve} = 1$ and $K_{Ve,\sigma} = 1$.

In Addition, Fig. 9 displays a comparison of the power factor of the Vernier and the pm machine. Besides the actual power factor, Fig. 9 also shows the power factor neglecting leakage effects. As already expected Fig. 9 confirms the huge impact of the leakage coefficients on the power factor. In this case, the Vernier coefficients (22), (24) continuously increase from 1.61 to 3.62 and from 4.22 to 6.44. Furthermore, Fig. 9 shows a very good agreement between the FEA and the presented analytic model. As this paper focuses on the power factor calculation for Vernier machines, the FEA only validates the model results for the Vernier machine.

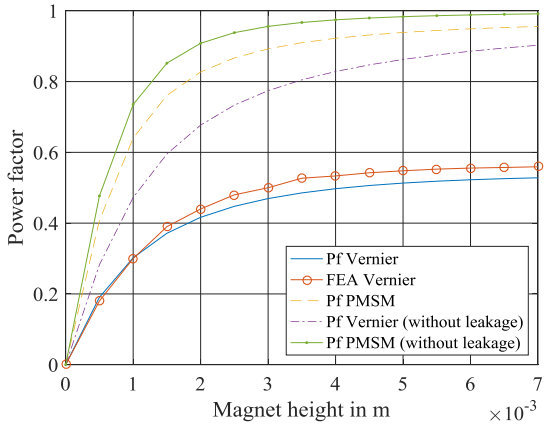

Fig. 9: Power factor for both machines with and without leakage effects

As the obtained q-inductances of Vernier and pm machine are in the same range, see Fig. 7, and the calculated no-load back-EMF of the Vernier machine is higher than the one of the pm machine, see Fig. 8, the poor power factor mainly originates from the higher electrical frequency in the Vernier machine. Assuming the same output speed, the electrical frequency of the Vernier machine is about the gear ratio

$$G_r = \frac{p_r}{p_s} \tag{25}$$

higher than in the pm machine. Since the no-load back-EMF is only slightly increased compared to a pm machine, a compensation of the higher electrical frequency is not possible in most cases and the power factor strongly decreases compared to a pm machine.

However, the presented analytic model shows additional geometric dependencies. Thus, considering a variation of the following parameters covers all simple geometric changes of the airgap structure: magnet height, FMP height, FMP width and stator tooth width. Therefore, Fig. 10 shows the power factor of the Vernier machine for various stator tooth widths and different FMP widths in a contour plot.

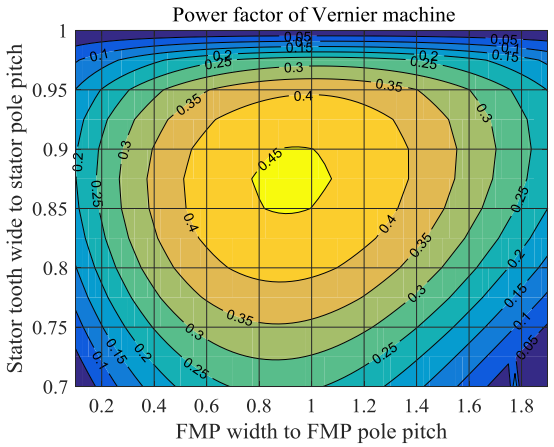

Fig. 10: Power factor for different FMP and stator tooth widths

The magnet height is 2.61 mm and the FMP height is 5.25 mm. Consequently, varying the stator tooth wide and the FMP width clearly shows that the best sector for the stator tooth width to the stator pole pitch ratio is 0.85 to 0.9. In addition, the best sector for the FMP width to the FMP pole pitch ratio is 0.8 to 1.1.

Furthermore, Fig. 11 presents the power factor of the Vernier machine for the variation of the magnet height and the FMP height in a contour plot. Therein, the stator tooth width to stator pole pitch ratio is 0.85 and the FMP width to FMP pole pitch ratio is 0.8.

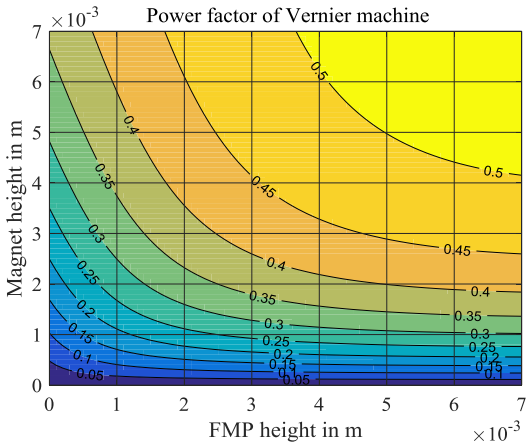

Fig. 11: Power factor for different FMP and magnet heights

Thereby, Fig. 11 indicates a steady improvement of the power factor while increasing both parameters. However, the improvement is very small compared to the design space used. Yet, choosing the magnet and the FMP height greater than 3 mm ensures a power factor above 0.4.

Moreover, Fig. 12 presents the power factor of the Vernier machine for different stator diameters.

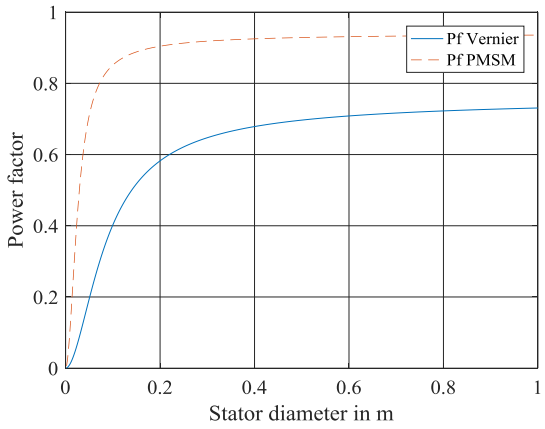

Fig. 12: Power factor for different stator diameters

A change of the stator diameter directly affects the pm machine coefficients (21), (23), though the stator diameter indirectly changes the FMP width b_{pp}, the width between two FMPs b_{air} and the stator tooth width b_s. However, Fig. 12 firstly shows a high gradient of the power factor for increasing stator diameters. Nevertheless, with increasing diameters the gradient of the power factor drops down. Consequently, it is difficult to maintain a good power factor for small Vernier machines with concentrated windings.

IV. Conclusion

This paper presents an analytic power factor model for Vernier machines with concentrated windings and different numbers of stator slots and FMPs. In contrast to the already derived models, the comparison to FEA results shows the necessity of considering the stator leakage flux in the q-inductance calculation. The presented model shows a very good accordance to the FEA and is simple and fast. However, the main uncertainty in generalizing the model is the identification of the leakage path. Furthermore, the parameter variation shows some optimal sectors for the stator tooth width and the FMP width. Nevertheless, improving the power factor above a certain level by simple airgap variations proves to be difficult. Besides, a variation of the stator diameter shows that the power factor is especially poor for very small machines.

References

[1] A. Toba and T. A. Lipo, "Generic torque-maximizing design methodology of surface permanent-magnet vernier machine," in *IEEE Transactions on Industry Applications*, vol. 36, no. 6, pp. 1539-1546, Nov/Dec 2000.

[2] S. L. Ho, S. Niu and W. N. Fu, "Design and Comparison of Vernier Permanent Magnet Machines," in *IEEE Transactions on Magnetics*, vol. 47, no. 10, pp. 3280-3283, Oct. 2011.

[3] R. Qu, D. Li and J. Wang, "Relationship between magnetic gears and vernier machines," *Electrical Machines and Systems (ICEMS), 2011 International Conference on*, Beijing, 2011, pp. 1-6.

[4] G. Liu, M. Chen, W. Zhao, Q. Chen and W. Zhao, "Design and Analysis of Five-Phase Fault-Tolerant Interior Permanent-Magnet Vernier Machine," in *IEEE Transactions on Applied Superconductivity*, vol. 26, no. 4, pp. 1-5, June 2016.

[5] D. Li, R. Qu and J. Li, "Topologies and analysis of flux-modulation machines," *2015 IEEE Energy Conversion Congress and Exposition (ECCE)*, Montreal, QC, 2015, pp. 2153-2160.

[6] L. Xu, G. Liu, W. Zhao, J. Ji and X. Fan, "High-Performance Fault Tolerant Halbach Permanent Magnet Vernier Machines for Safety-Critical Applications," in *IEEE Transactions on Magnetics*, vol. 52, no. 7, pp. 1-4, July 2016.

[7] B. Kim and T. A. Lipo, "Operation and Design Principles of a PM Vernier Motor," in *IEEE Transactions on Industry Applications*, vol. 50, no. 6, pp. 3656-3663, Nov.-Dec. 2014.

[8] B. Kim and T. A. Lipo, "Analysis of a PM Vernier Motor With Spoke Structure," in *IEEE Transactions on Industry Applications*, vol. 52, no. 1, pp. 217-225, Jan.-Feb. 2016.

[9] M. Seilmeier, S. Ebersberger and B. Piepenbreier, "PMSM model for sensorless control considering saturation induced secondary saliencies," *2013 IEEE International Symposium on Sensorless Control for Electrical Drives and Predictive Control of Electrical Drives and Power Electronics (SLED/PRECEDE)*, Munich, 2013, pp. 1-8.